Unravelling the nature of H-mode access at ASDEX Upgrade and TCV using gyrokinetic simulations

B. J. Frei[1,*], R. Bilato[1], W. Zholobenko[1], O. Grover[1], M. Bergmann[1], P. Ulbl[1], F. Jenko[1], S. Rienaecker[2], L. Vermare[2], P. Hennequin[2], and B. Labit[3]

[1] *Max-Planck-Institut für Plasmaphysik, 85748 Garching, Germany*

[2] *Laboratoire de physique des plasmas, CNRS-École polytechnique, 91128 Palaiseau, France*

[3] *EPFL, Swiss Plasma Center, CH-1015 Lausanne, Switzerland*

In tokamaks, the direction of the ion ∇B drift relative to the active X-point defines the *favourable* (*fav*) and *unfavourable* (*unfav*) drift configurations. Reversing this direction strongly influences the high-confinement (H-mode) power threshold, with *unfav* discharges generally requiring more than twice the threshold power of *fav* ones [1]. This difference, observed across multiple devices, experimentally correlates with a deeper radial electric field (E_r) well near the separatrix in *fav* prior to the low-to-high (L–H) confinement transition. Understanding the mechanism underlying this E_r asymmetry is crucial for ITER and future reactors, as it determines the required heating power and limits operational flexibility. Experimental evidence indicates that the E_r shear facilitates H-mode access in *fav*, while it is weaker in *unfav* [1]. Since neoclassical (NC) effects alone cannot account for the observed E_r asymmetry between *fav* and *unfav*, turbulence must play a significant role in the self-consistent interplay between transport, equilibrium profiles, flows, and E_r. Capturing this interplay requires a first-principles, nonlinear, gyrokinetic (GK) treatment of edge and scrape-off layer (SOL) turbulence in realistic diverted geometry. Here, we present such an investigation for *fav* and *unfav* L-mode discharges with matched parameters at AUG and TCV. We identify the nonlinear mechanism that sets the depth of the E_r well as the nonlinear energy transfer from turbulence to mean (zonal) poloidal flows driven by the radial gradient of the total velocity-stress.

We model the discharges using the spectral version of the full-f, electromagnetic, long-wavelength and collisional GK code `GENE-X` [2, 3, 4], which evolves edge and SOL turbulence with X-points in realistic diverted geometry. At AUG, we consider a dedicated matched pair of lower single-null deuterium discharges, #36983 (*fav*) and #37375 (*unfav*) [1], with $n_e \simeq 2.7 \times 10^{19}$ m^{-3}, $|B_\phi| = 2.5$ T, $|I_p| = 0.8$ MA, and 600 kW of ECRH in L-mode. To minimise differences between the two configurations, the *unfav* equilibrium is obtained by reversing only the direction of B_ϕ, which inverts the ion ∇B drift and the magnetic helicity while leaving the geometry otherwise unchanged. A radially localised density source near the separatrix mimics neutral ionisation, and both simulations are performed until a quasi-steady state

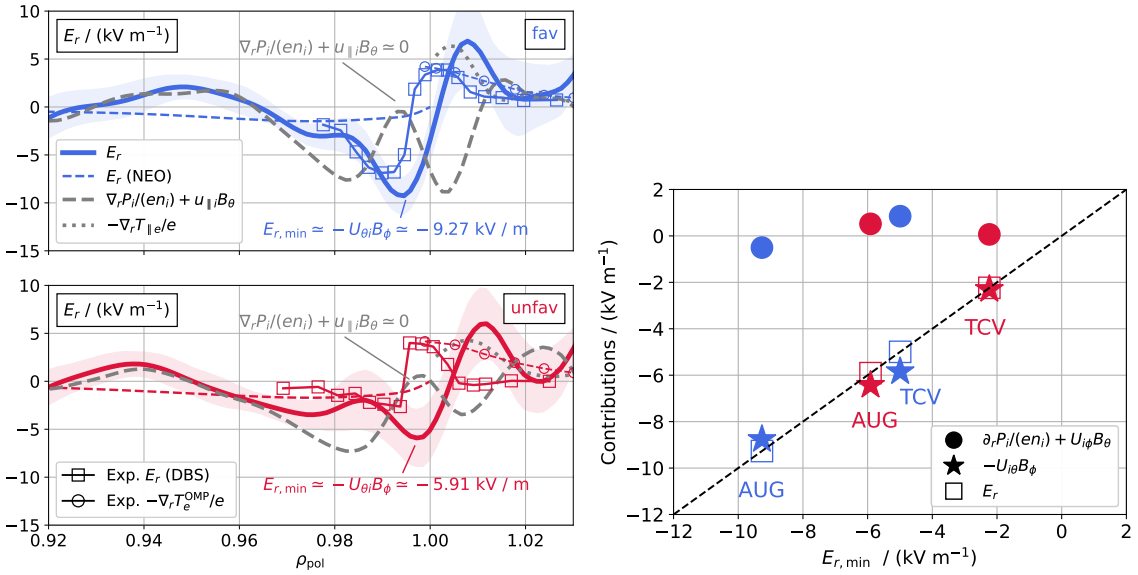

Figure 1: **Left:** OMP E_r from `GENE-X` (solid) in *fav* (top) and *unfav* (bottom) at AUG. Shading indicates the standard deviation. DBS measurements [1] are shown as squares; the NC E_r (NEO, using `GENE-X` profiles) is dashed; SOL estimates from experiment ($-\nabla T_e^{\mathrm{OMP}}/e$, circles) and GK theory ($-\nabla T_{\|e}/e$, dotted) are also shown. **Right:** Contributions to the E_r well minimum ($E_{r,\min}$) from the radial force balance, plotted against $E_{r,\min}$ for AUG and TCV in *fav* and *unfav*.

is reached. The same setup is applied to a matched pair of Ohmic L-mode TCV discharges, #86594 (*fav*) and #86593 (*unfav*). In `GENE-X`, E_r is obtained directly from the self-consistent GK quasi-neutrality condition [3, 4] and therefore contains both the short wavelength turbulent and long wavelength NC contributions self-consistently.

The simulated outboard midplane (OMP) profiles of density (n_e), electron and ion temperatures (T_e and T_i), and the self-generated toroidal velocity ($U_{\phi i}$) agree well with experiments at both AUG and TCV and, consistent with experiments, are nearly insensitive to the ion ∇B drift direction. In contrast, the simulated E_r profiles reproduce the experimentally observed asymmetry: the E_r well near the separatrix is significantly deeper in *fav* than in *unfav* (Fig. 1a), even though n_e, T_i, and $U_{\phi i}$ are essentially identical in the two cases. Further inside the edge ($\rho_{\mathrm{pol}} \lesssim 0.98$) and in the SOL, E_r is similar between *fav* and *unfav*. Comparison with NC predictions (NEO) shows that the amplitude of the poloidal velocity $U_{\theta i}$ is consistent with NC only in *unfav*: in *fav* its amplitude near the separatrix substantially exceeds the NC level, highlighting an additional, non-NC drive. The deeper well yields an inner $E \times B$ shear about 1.6 times stronger in *fav*.

The origin of the E_r asymmetry is identified through the ion radial force balance, $E_r = \nabla_r P_i/(q_i n_i) + U_{\phi i} B_\theta - U_{\theta i} B_\phi$ [4]. The diamagnetic and toroidal-rotation terms nearly cancel

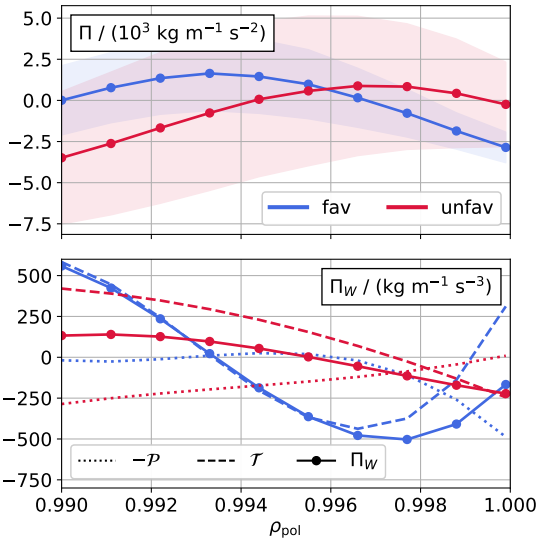

Figure 2: **Top:** time-averaged radial profiles (with standard deviations) of the total velocity stress Π in *fav* (blue) and *unfav* (red) at AUG. **Bottom:** radial profiles of the stress work Π_W (solid), its turbulent-transport ($\mathscr{T}$, dashed) and production ($-\mathscr{P}$, dotted) contributions, $\Pi_W = \mathscr{T} - \mathscr{P}$.

within the E_r well, such that $E_{r,\min} \simeq -U_{\theta i} B_\phi$. As a consequence, the depth of the E_r well is set by the poloidal flow $U_{\theta i}$, which is much larger in *fav*. Since the OMP profiles and toroidal rotation are similar between *fav* and *unfav*, this difference cannot originate from NC physics but must arise from nonlinear turbulence–flow interaction [5].

Inside the E_r well, the poloidal flow is dominated by the $E \times B$ velocity, $U_{\theta i} \simeq u_\theta$ (with u_θ the poloidal component of $E \times B$ velocity u). An evolution equation for the flux-surface-averaged (FSA, zonal) poloidal momentum density follows from the GK vorticity equation, yielding $\partial_t \langle M u_\theta \rangle = -d_r \Pi + \Lambda$, where M is the total mass density and $\Pi = \langle M \rangle \langle\langle u_\theta u_r \rangle\rangle$ is the total (electrostatic) velocity stress [5], a full-f generalisation of the Reynolds stress $\mathscr{R}$ written with the Favre average $\langle\langle f \rangle\rangle = \langle M f \rangle / \langle M \rangle$. Λ represents NC viscosity damping. Beyond $\partial_r \mathscr{R}$, Π additionally captures radial turbulent transport of poloidal momentum, poloidal density asymmetries, and triple fluctuation correlations. A negative radial gradient of Π accelerates the poloidal flow.

In *unfav*, the weak $E \times B$ flow is directed towards the X-point and the eddies are tilted mainly by magnetic shear, so Π varies little radially and its gradient is small. In *fav*, the stronger $E \times B$ flow is directed away from the X-point and reinforces the eddy tilt [6], modulating the poloidal distribution of Π and producing a finite, self-amplifying gradient. As a result, the negative radial gradient of Π around the E_r well is much larger in *fav* than in *unfav* (Fig. 2, top).

The efficiency of the energy transfer from turbulence into the mean (zonal) poloidal flow is quantified by the FSA poloidal kinetic energy, $K_\theta = \langle M u_\theta \rangle^2/2$, and is driven by the stress work $\Pi_W = \langle\langle u_\theta \rangle\rangle \, d_r \Pi = \mathscr{T} - \mathscr{P}$, with $\mathscr{T}$ the turbulent transport of mean kinetic energy and $\mathscr{P}$ the production by turbulence. As shown in Fig. 2 (bottom), Π_W is much larger (in amplitude) around the E_r well in *fav*, where $\mathscr{T}$ dominates inside the E_r well and $-\mathscr{P}$ near the separatrix. In *unfav*, $\mathscr{T}$ and $\mathscr{P}$ both remain small. The energy transfer mediated by Π_W thus provides the poloidal-flow acceleration that shapes the deeper E_r well in *fav*. Conversely, the fluctuation Fourier spectra show systematically higher amplitudes in *unfav*, while the frequency–wavenumber relations and phase shifts remain similar. The ion ∇B drift direction therefore primarily influences the turbulence intensity (larger in *unfav*) and the turbulence–flow energy transfer (stronger in *fav*).

The same picture holds at TCV: the simulations reproduce the deeper E_r well in *fav*, with $E_{r,\min} \simeq -U_{\theta i} B_\phi$ set again by the non-NC poloidal flow. The associated Π_W is larger in *fav*. Decomposing $E_{r,\min}$ confirms that, in all four cases (AUG and TCV, *fav* and *unfav*), the poloidal-flow term, $-U_{\theta i} B_\phi$, alone sets the depth of the E_r well (Fig. 1, right). Larger fluctuation levels in *unfav* are also observed. The radial correlation length of density fluctuations is reduced across the outer shear layer in *fav*, where the E_r shear is at least twice as large as in *unfav*. Finally, flux-driven simulations are performed demonstrating the stronger deepening of E_r in *fav* when the input power and edge density source are suddenly increased.

To summarize, first-principles and full-f GK simulations in diverted geometry reproduce the experimentally observed deeper E_r well in *fav* at both AUG and TCV, experimentally associated with the lower H-mode power threshold in *fav*. Turbulence-driven poloidal flows—arising from enhanced nonlinear turbulence–mean-flow energy transfer driven by the radial gradient of the full-f velocity stress Π— are identified as the key mechanism setting the depth (and shear) of the E_r well. This transfer is enhanced in *fav* and strongly reduced in *unfav* depending on the orientation of the localised $E \times B$ shear relative to the X-point. Turbulence intensity is simultaneously higher in *unfav*. Within the turbulence–flow-shear suppression paradigm, the deeper E_r well and the reduced turbulence in *fav* provide a self-consistent, validated explanation for the lower H-mode power threshold in *fav*. Flux-driven simulations aimed at triggering the L–H transition [7] are required to test this mechanism against measured L–H power thresholds.

References

[1] U. Plank *et al.*, Phys. Plasmas **30**, 042513 (2023)

[2] D. Michels *et al.*, Comput. Phys. Comm. **264**, 107986 (2021)

[3] B. J. Frei *et al.*, Comput. Phys. Comm. **316**, 109817 (2025)

[4] B. J. Frei *et al.*, Nucl. Fusion **65**, 116026 (2025)

[5] B. J. Frei *et al.*, accepted in Phys. Rev. Lett. (2026)

[6] O. Grover *et al.*, Nucl. Fusion **64**, 056020 (2024)

[7] W. Zholobenko *et al.*, Phys. Rev. Lett. (2026)

*Correspondence: baptiste.frei@ipp.mpg.de